New structure and spin state of iron-rich $(Mg,Fe)SiO_3$ post-perovskite

2010 J. Phys.: Conf. Ser. 215 012100

(http://iopscience.iop.org/1742-6596/215/1/012100)

New Structure and Spin State of Iron-Rich $(Mg,Fe)SiO_3$ Post-Perovskite

T. Yamanaka[1], W. L. Mao[2], H-K Mao[1], R.J. Hemley[1] and G. Shen[3]

[1] Geophysical Laboratory, Carnegie Institution of Washington, 5251 Broad Branch Rd. NW Washington DC
[2] Department of Geological and Environmental Sciences, Stanford University, Stanford, CA 94305
[3] HPCAT, Advanced Photon Source, Argonne National Laboratory, Argonne, IL 60439

E-mail t.yamanaka@kce.biglobe.ne.jp

Abstract There was a discrepancy between the seismic tomography and the elastic property of $MgSiO_3$ perovskite at near the D'' zone and core boundary. Since a discovery of post-perovskite (ppv) of $MgSiO_3$, many investigations have made to explain the presence of low seismic velocity of the lower mantle and D'' zone. However, precise experimental structure analysis of ppv-$(Mg_{1-x}Fe_x)SiO_3$ has never been reported because of the experimental difficulty. Fe and Mg cation distribution and ordering in ppv-$(Mg,Fe)SiO_3$ in consideration of spins states are significant subject in lower mantle electronic and magnetic states. The present experiment aims X-ray emission study and structure analysis by Rietveld profile fitting of ppv-$(Mg_{0.6},Fe_{0.4})SiO_3$ by the precise powder diffraction measurement. Monte Carlo calculation proposed the reliable structures of iron-rich phase of ppv-$(Mg,Fe)SiO_3$: *Pmmn*, *Pmma*, and *Cm2m* and *Cmcm* proposed by. The best-fit structure model with the highest reliability in the Rietveld fitting of ppv-$(Mg_{0.6}Fe_{0.4})SiO_3$ is the structure of space group *Pmma*, in which Fe and Mg occupy two different sites of M1 and M2: the site occupancies are $(Fe_{0.25}Mg_{0.75})$ in the larger M1 site and $(Fe_{0.55}, Mg_{0.45})$ in the smaller M2 site.. The two-site model is consistence with the previous results of X-ray emission and X-ray Mössbauer experiments..

Introduction

Before a discovery of the $CaInO_3$ of *Cmcm* structure as post-perovskite (ppv) of $MgSiO_3$ in 2004, there was a discrepancy between the seismic tomography and the elastic property of $MgSiO_3$ perovskite at near the D'' zone. The ppv was proposed by simulation of the powder diffraction pattern[1] and the first-principle calculation[2-3], numerous high-pressure experiments of $MgSiO_3$ ppv have been undertaken to explain the anomalous seismic phenomena observed in D'' zone.[4-10]

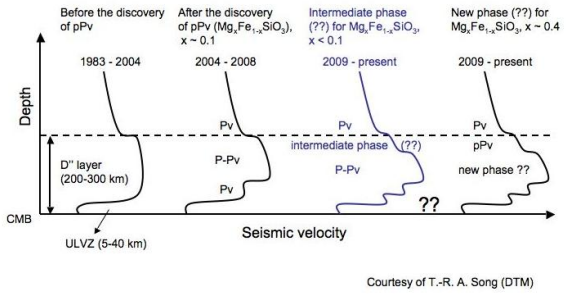

Figure 1. Schematical drawing of the seismic velocity neat the mantle–core boundary.
Possible seismic velocity based on the seismic tomography is represented before and after the discovery of ppv. New intermediate seismic phase has been found recently.

The near core-mantle boundary (CMB) with ultra low seismic velocities was explained by silicate ppv containing up to 40 mol% $FeSiO_3$ (En60), which has a low shear wave velocities and high Poisson's ratio[5].

In situ synchrotron X-ray diffraction measurements[11] at high-pressure and -temperature in a laser-heated diamond anvil cell (DAC) from 1640 to 4380 K at 119–171 GPa show a precise post-perovskite phase transition boundary and the depths of paired seismic discontinuities at CMB pressure. Recently a new anomaly of the seismic velocity of the Earth's D'' layer is found in the local areas by seismic tomography. The seismic velocity vs depth is schematically drawn in **Fig.1**.

Rietveld structure analyses of ppv of several ppv compounds with space group *Cmcm* have been reported and their equation states were also reported based on the $CaInO_3$ structure model.[12-13] Many higher-pressure phases of perovskite compounds, ppv-ABO_3 have been reported by X-ray powder diffraction studies,[14-17] neutron diffraction study[18] and first principles calculation based on density functional theory.[19-20] The low shear wave velocities using

iron-rich post-perovskites $(Mg_{0.6},Fe_{0.4})SiO_3$ (En60) were investigated to disclose the seismic velocity at boundary layer between crystalline silicate lower mantle and liquid iron outer core.[21] Thermoelastic properties of ppv-$(Mg_{0.91}Fe_{0.09})SiO_3$ up to 135 GPa and 2,700 K were reported.[22]

Structure refinements of ppv-$(Mg_{1-x},Fe_x)SiO_3$ solid solutions have never been carried out because of experimental difficulties. Fe and Mg cation distribution and ordering in the ppv-$(Mg_{1-x},Fe_x)SiO_3$ structure are a significant factor in lower-mantle equillibria and the equation of state. Several papers proposed different type of ppv structures from $CaInO_3$ structure. Rietveld refinement of ppv-$NaMgF_3$ structure was a better fit to $Cmc2_1$, which is a non-isomorphic subgroup of *Cmcm* of the structure of $CaIrO_3$[13]. However, the model cannot produce the two-site model for eight-fold cation sites. In comparison with the structural features, ppv-$MgSiO_3$ is more similar to ppv-$MgGeO_3$, and ppv-$NaMgF_3$ than ppv-CaIrO3.16 Further aluminous magnesium metasilicate ppv is inconsistent with the $CaIrO_3$ structure from X-ray diffraction data and Raman spectra studies.[23] Finite temperature, minor element chemistry, kinetics of phase transformation and actual stress regime are plausible reasons for the observed differences from the previously reported ppv phases. Previous X-ray Mössbauer spectroscopic study of ppv-$(Mg_{0.6},Fe_{0.4})SiO_3$ showed two doublets of ferrous cations.[24] The study proves the two-site model of ferrous ions in the ppv structure is different from $CaInO_3$ structure which has a one-site model.

The present experiment aims the Rietveld profile fitting of iron-rich magnesium meta-silicate ppv-$(Mg_{0.6},Fe_{0.4})SiO_3$ by the precise powder diffraction measurement at 137 GPa with laser heating at about 2000 K. Above 136 GPa of the transition pressure "D" zone, spin state of ferrous ion has been clarified by the X-ray emission experiment.

Powder diffraction experiment and structure analysis

The sample of ppv-$Mg_{0.6}Fe_{0.4}SiO_3$ (En60) has been prepared on the beamline from the starting material of pyroxene phase. The fine powder sample and platinum internal pressure marker were loaded into a rhenium gasket which was preindented to 40 μm. The sample was compressed to 130 GPa and then heated to 2000 K on the beamline by the double-sided Nd:YLF laser-heating system using the beveled diamond-anvils of 90 μm culets and 450 μm outer diameter. Temperature was determined by spectral radiometry based on the Planck radiation function. Pressure was determined using the Pt equation of state.

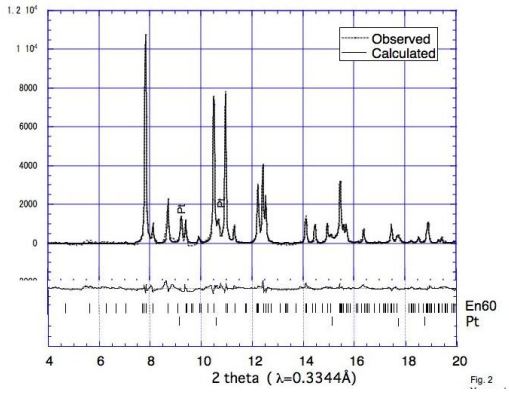

Figure 2. Rietveld profile fitting of ppv-$(Mg_{0.6}Fe_{0.4})SiO_3$. The observed data (dotted line) taken at 137 GPa after quenching sample from 2000 K is presented by solid line. The residual peaks of I_{obs}-I_{cal}c are presented in the lower level. The bars indicate the calculated peak positions of sample (En60) and the Pt pressure marker.

Powder diffraction experiments were executed at the Advanced Photon Source (APS) at Geo Soil Enviro CARS (GSECARS) 13-ID-D, and at the High Pressure Collaborative Access Team (HPCAT) 16-ID-B. These beam lines are described.[25] Powder diffraction pattern were collected by imaging plate at HPCAT, and by CCD at GSECARS. The diffraction patterns were processed and digitized with FIT2D program.[26]

After conversion from pyroxene to ppv phase, we collected twenty patterns at different locations of sample over the entire laser-heated area at several different omega angles in order to avoid the non-uniformity in diffraction patterns due to the preferred orientation and grain growth by laser heating in the gasket. A monochromatic X-ray beam with λ = 0.3344 Å were used for incident beam. The beam was focused down to 5 x 7 μm through DAC and

impinged on the sample. The final pattern represents the sum of all spectra from different areas. The standard deviation in integrated intensity was less than 3%.

We tried to determine the most reliable structure of post-perovskite polymorph of $(Mg,Fe)SiO_3$ from the possible structure models, which were provided by the Monte Carlo calculation. The calculation was executed using the diffraction intensities and reflection indices obtained by the indexing process. Rietveld profile fittings for the four possible structure models of *Pmmn*, *Pmma*, *Cm2m* and *Cmcm* have been undertaken for least-squares refinement. Initial atomic positional parameters in the refinement are applied from the Monte Carlo calculation.

Rietveld profile fitting was conducted by program RIETAN-2000.[27] The variable parameters in the profile fitting are background, scale factor, pseudo-Voigt profile function including FWHM and asymmetry parameters, besides the structure parameters, lattice constants, atomic positional coordinates, site-occupancy parameter and temperature factors. First the background intensity distribution was adjusted for the refinement. Lattice constants and atomic positional coordinates were set to the variable parameters and subsequently profile parameter and site-occupancy parameters were varied in the refinement procedure. Finally full matrix least-squares refinement was conducted.

X-ray emission spectroscopy experiment.

X-ray emission spectra (XES) measurement has confirmed the high-low spin transition under the condition of the "D" zone. The synthesized sample was compressed to 124 GPa and heated to 1800 K at BL16-ID-B of HPCAT, APS. The incident X-ray beam was focused using a pair Kirkpatrick-Baez mirrors. A spherically bent Si (333) crystal was used for the energy analyzer, which sits along with the detector on a high resolution (0.5 eV). The Fe-$K\beta$ emission spectrum is collected through the gasket. Changing the analyzer angle θ and simultaneously detector angle 2θ of Rowland-circle spectrometer scans energy. In order to reduce absorption by air, helium gas was filled in the X-ray path. The detailed specification was reported in our previous papers.[28, 29]

Result

The Monte Carlo calculation yields four reasonable structure models with different cation distributions by four space groups of $MSiO_3$: *Pmmn* (*Pmnm*) for $(M1,M2)[Si]O_3$, *Pmma* (*Pmcm*) for $(M1, M2)[Si1,Si2]O_3$, *Cm2m* for $(M1,M2)[Si]O_3$ and *Cmcm* for $(M1)[Si]O_3$. The space group $Cmc2_1$ proposed for ppv-$NaMgF_3$ [11] is not the candidate for the two-site model. First three models belong to the non-isomorphic subgroups of *Cmcm*.[30]

The structure model of space group *Pmma* shows the highest reliability parameters in the least-squares fitting in the Rietveld refinement. For comparison, both results based on *Pmma* and *Cmcm* are presented in **Table 1**. Rietveld refinement based on the $CaInO_3$ structure (*Cmcm*) model did not provide the best fit to the powder diffraction intensity of ppv-$(Mg_{0.6}Fe_{0.4})SiO_3$ (ppv-En60).

Note that *Pmma* is same symmetry as *Pmcm*. The difference between *Pmma* and *Cmcm* is only their lattice types. Both reliability factors, RI (intensity fitting) and RF (structure factor fitting), of the former model are better than those of the latter. The result of Rietveld refinement of both *Pmma* and *Cmcm* are presented in **Fig. 2**, which indicates the *Pmma* model gives much better fit to the observed intensity distribution than the *Cmcm* model. The converged lattice constants are a=6.1252(7) Å, b=2.4648(3) Å, c=8.1529(10) Å. The lattice constants are naturally same as those taken from the *Cmcm* model. There are two different sites M1 (2*e*) and M2 (2*f*) in the *Pmma* model and both have the site symmetry *mm*2. On the other hand Fe and Mg cations are randomly distributed in only one site M (4*c*) in *Cmcm* with the site symmetry *m*2*m*. These cations are partly ordered in two sites, M1 and M2 in

Pmma model, the former site occupancy is ($Mg_{0.75}$ $Fe_{0.25}$) and the latter ($Mg_{0.45}$ $Fe_{0.55}$) by the site occupancy refinement. About 70% of Fe atoms occupies at the M2 site. The over all temperature parameters are also converged to the reasonable values for all atoms. Si atoms locate the two sites, (2*a)* and (2*d*) with the site symmetry of .2/*m*.

Table 1 positional paprameters

Space group *Pmma* (SG=51) Z=4

atom	Wyc	x	y	z	B
M1	2*e*	0.25	0.0	0.255(4)	2.3(0.7)
M2	2*f*	0.25	0.5	0.751(8)	3.6(0.1)
Si1	2*a*	0.0	0.0	0.0	2.8(0.8)
Si2	2*d*	0.0	0.5	0.5	1.0(0.7)
O1	2*e*	0.25	0.0	0.920(8)	1.6(0.8)
O2	2*f*	0.25	0.5	0.435(7)	2.6(0.9)
O3	4*i*	0.441(4)	0.0	0.639(4)	0.5(0.9)
O4	4*i*	0.437(8)	0.5	0.119(4)	1.8(1.3)

RI = 6.90 RF = 6.28 Rwp = 0.25 Rp = 0.16 s = 0.6183
M1 (Fe0.25 Mg0.75) M2 (Fe0.55 Mg0.45)
a=6.1252(7) *b*=2.4648(3) *c*=8.1529(10) Vol=123.09(3)

Space group *Cmcm* (SG=63) Z=4

atom	Wyc	x	y	z	B
M	4*c*	0.0``	0.253(7)	0.25	3.0(0.2)
Si	4*a*	0.0	0.0	0.0	1.7(0.2)
O1	4*c*	0.0	0.928(2)	0.25	2.7(0.3)
O2	8*f*	0.0	0.636(1)	0.439(1)	0.3(0.3)

RI = 8.34 RF = 6.62 Rwp = 0.26 Rp = 0.15 s = 0.6312
M (Fe0.40 Mg0.60)
a=2.4647(3) *b*=8.15345(11) *c*=6.1257(8) Vol=123.10(2)

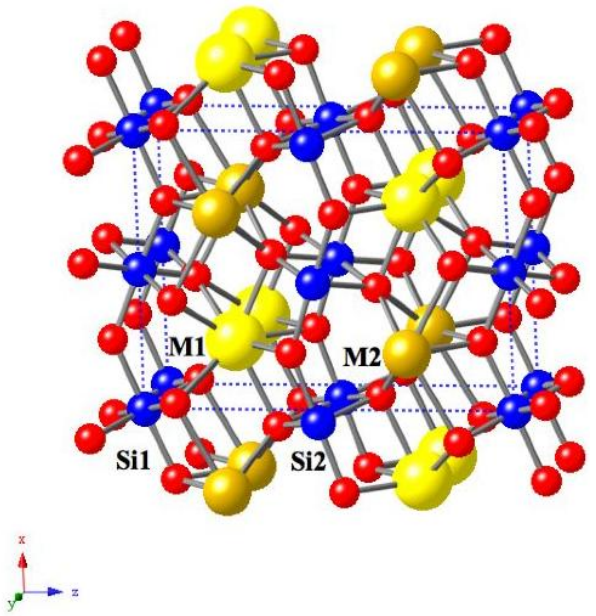

Figure 3. Structure of post- perovskite $Mg_{0.6}Fe_{0.4}SiO_3$ with the space group of *Pmma.*
Atoms are represented by red for O^{2-}, blue for Si^{4+}, brown for M1 $(Fe_{0.25}Mg_{0.75})^2$ and yellow for M2$(Fe_{0.55}Mg_{0.45})^2$.

The bond distances were calculated in the both models of *Pmma* and *Cmcm.* M1 and M2 cations are eight-fold coordinated and form the almost anti-dipyramid, as shown in **Fig. 3**. Si atom has a six-fold coordination. Oxygen atoms at the O1 and O2 sites have a four-fold coordination. On the other hand oxygen at the O3 and O4 sites five-fold. The average bond-distance of M1 is larger than that of M2 in the former model. The ionic radius of $^{VIII}Fe^{2+}$ (0.92 Å) is larger than $^{VIII}Mg^{2+}$ (0.89 Å) at ambient conditions with reference to the empirical ionic radii.[31] In general, the average values are consistent with the cation radii. However, the large M1 site of ppv-En60 is more occupied by the smaller Mg^{2+} and the seemingly larger Fe^{2+}occupies the small M2 site. This is because Fe^{2+}in the M2 site is the low-spin state, which reduces the ion radius to 0.74 Å. Consequently Fe^{2+} becomes smaller than Mg^{2+}. These two sites are distributed alternatively and keep a zigzag mode in the direction of *a*. axis, as seen in **Fig. 3**.

Bond distances indicate the smaller M2 site is more distorted than the M1 site. The inter planer distance in the direction of the *z* axis between two oxygen layers of the M2 molecule is about 10% shorter than that of M1 by the compression under megabar. The M2 site is more distorted than the M1 site and the large distortion of the M2 site is consistent with the quadruple splitting found the Mössbauer spectroscopic study.[24]

Discussion

Numerous experiments and calculations have discussed electron spin transitions and magnetic spin transitions of the interiors of low mantle and D" zone.[24, 32-35] The present structure refinement of ppv-$(Mg_{0.6}Fe_{0.4})SiO_3$ is in accordance with the Mössbauer experiment and X-ray emission study. The emission spectroscopy under high pressure can detect the spin transition. The local environment of the Fe^{2+} site of the M1 and M2 sites is in the eight-fold anti-pyramid symmetry in the ppv structure. The electronic spin have the energy levels of electronic state, $d_{x^2-y^2} > d_{z^2} > d_{xy} > d_{yz} \fallingdotseq d_{xz}$. Six *d*-electrons of Fe^{2+} follow the Hunt rule in the HS state at low pressure. At the extremely high-pressure condition, the atomic configurations by the compression in the direction of *z* of the molecular axis (parallel to the z axis in *Pmma* setting) makes the LS state: anti-parallel spin pairs by the Pauli principle in d_{xy}, d_{yz} and d_{xz} spin state in the eight-fold coordination sites, as shown in **Fig. 4**.

We investigated two models in both HS and LS states. One model is composed of perfectly ordered cation distribution, Mg at the M1 site and Fe at the M2 site, with the anti-ferromagnetic arrangement along the longest diagonal of the unit cell. This characterize two unequivalent sites with a larger fraction of iron at M2 than at M1 giving a space group of *Pmma*. Another model is a disordered distribution of Fe and Mg at the M1 and M2 site with the anti-ferromagnetic symmetry along the y-axis. This model has the same amount of Fe in the M1and M2 sites, which produces the structure of *Cmcm*.

Additionally we have found that the *Pmma* structures undergo a high to low spin transition as the pressure is increased. This suggests that the HS state is stabilized by keeping the Fe atoms as far apart from each other as possible, allowing both for an increased relaxation of the surrounding structure and minimizing the spin-spin interaction between the iron sites. This results in the much higher transition pressure of the *Pmma* phase. This is consistent with the diffraction experimental finding of the *Pmma* phase, which has an increased average distance between the Fe atoms compared to the disordered *Cmcm* structure. Theoretical studies should focus on the discrepancy of the spin transition pressures between our calculation of the *Pmma* phase which finds that a HP state persists until about 410 GPa and the experimental finding that the iron rich site is in a LS state at the experimental pressure of 137 GPa.

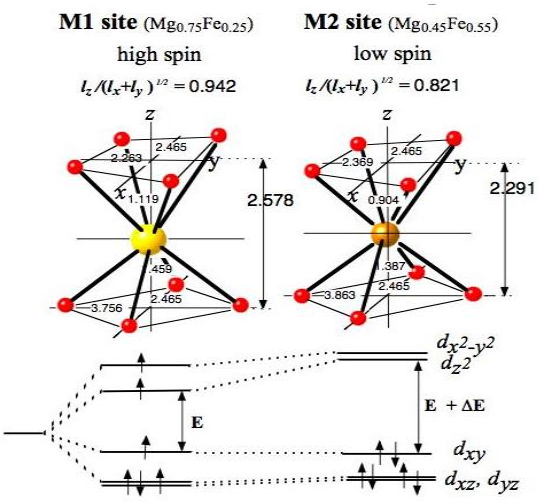

Figure 4. Deformation of the M1 and M2 sites and their electronic
spin configuration. The atomic configuration and site symmetry of the M1 and M2 site are presented. An average bond length of the M1 site for $Fe_{0.25}Mg_{0.75}$ and M2 for $Fe_{0.50}Mg_{0.50}$ have an average bond length of 1.9645 Å and 2.0276 Å. Fe^{2+} in the former site is in the HP state. On the other hand, that in the latter in the law-spin state. The M1 site is more distorted than the M2 site.

The present investigations cannot convince that the two-site model is only for iron-rich magnesium metasilicates. $MgSiO_3$ may have the two site structure of *Pmma* instead of *Cmcm* structure.. If it is not the case, the *Pmma* structure is the new structure and the phase boundary in the solid solution $(Mg_{1-x}Fe_x)SiO_3$ has to be determined. More data analyses based on the precise powder diffraction measurements under extreme high-pressure and high-temperature conditions have to be performed to solve these problems.

Conclusion

Search the possible candidates of ppv structure with the symmetries in the maximal non-isomorphic subgroups of *Cmcm*. Monte Carlo calculation was carried out using the diffraction intensities to find possible structure models.

Four reasonable space group symmetries of ppv structure with different cation distributions are found: *Pmmn* $(M_1, M_2)[Si]O_3$, *Pmma* $(M_1, M_2)[Si_1, Si_2]]O_3$, *Cm2m*, $(M_1, M_2)[Si\ ]O_3$, *Cmcm* $(M)[Si\ ]O_3$. Rietveld profile fitting experiments for these four candidates were carried out including variable site occupancy of Fe and Mg in M1 and M2 sites. The most reasonable structure is determined to be *Pmma* by reasonable bond distances, angles and temperature factors. Iron-rich post-perovskite has a new post perovskite structure of *Pmma* different from *Cmcm* (CaIrO3) structure.

Reference

1 Murakami, M., Hirose, K., Kawamura, K., Sata, N., Ohishi, Y., 2004. Science **304**, 855–858.
2 Tsuchiya, T., Tsuchiya, J., Umemoto, K., Wentzcovitch, R.M. 2004, Earth Planet. Sci. Lett. **224**, 241–248.
3 Oganov A. R. and Ono, S., 2004, PNAS 102, 10828-10831.
4 Shim, S.-H., Duffy, T. S., Jeanloz, R., & Shen, G.2004, *Geophys. Res. Lett.* **31**, L1060 2004.
5 Mao, W.L., Shen, G., Prakapenla, V.B., Meng, Y., Campbell, A.J., Heinz, D.L., Shu, J. Hemley, R.J. and Mao, H.K. 2004, PNAS 101, 15867-15869.
6 Helmberger, D., Lay, T., Ni, S., & Gurnis, M. 2005, *Proc. Nat. Acad. Sci.* **102**, 17257–17263.
7 Holzapfel, C., Rubie, D.C., Frost, D.J. and Langenhorst, F. 2005. Science **309**, 1707-1710.
8 Hirose, H. and Lay, T. 2008, Elements **4**, 183-189.
9 Tateno, S., Hirose, K., Sata, N. and Ohishi, Y. 2009, Earth and Planetary Science Letters **277**, 130–136
10 Fiquet, G., Guyot, F. and Badro, J. 2008, Elements **4**, 177-182.
11 Hutko, A.R., Lay, T., Revenaugh, J. and Garnero, E.J. 2008, Science **320**, 1070-1074.
12 Shieh, S.R., Duffy, T.S., Kubo, A., Shen, G., Prakapenka,V.B., Sata, N., Hirose, K. and Ohishi, Y. 2006, PNAS **103**, 3039-3043.
13 Ballaran,T,B., Tronnes, R.G. and Frost, D.J. 2007, American Mineralogist **92**, 1760-1763.
14 Hirose, K., Kawamura, K., Ohishi, Y., Tateno, S., Sata, N. 2005, Am. Mineral. **90**, 262–265.
15 Martin, C.D. Crichton, W.A., Liu, H., Prakapenka, V., Chen, J. and J. Parise, B. 2006, American Mineralogist **91**, 1703-1706.
16 Kojitani, H., Shirako, Y. and Akaog, M. 2007, Physics of the Earth and Planetary Interiors **165**,127–134.
17 Kubo, A., Kiefer, B., Shim, S.H., Shen, G., Prakapenka, V.B. and Duffy, T.S. 2008, American Mineralogist **93**, 965-976.
18 Martin, C.D., Smith, R.I., Marshall, W.G. and Parise, B. 2007, American Mineralogist **92**, 1912-1918.
19 Tsuchiya, T. and Tsuchiya, J.,. New high-pressure phase relations in $CaSnO_3$. American Mineralogist, **91**, 1879-1887 (2006).
20 Umemoto, K. and Wentzcovitch, R.M., Prediction of an U_2S_3-type polymorph of Al_2O_3 at 3.7 Mbar. PNAS **105**, 6526-6530 (2008)
21 Mao, W.L., Mao, H.K., Sturhahn, W., Zhao, J., Prakapenka, V.B., Meng,Y., Shu, J., Fei, Y. and Hemley, R.J. 2006, Science **312,** 564-565.
22 Shim, S.H., K. Catalli, K., Hustoft, J., Kubo, A., V. Prakapenka, V.B., Caldwell, W.A. and M. Kunz, M. 2008, PNAS **105**, 7382-7386.
23 Tschauner, O., Kiffer, B., Liu, H.Z., Sinogeikin, S., Somayazulu, M. and , Luo, S.N. 2008, American Mineralogist, **93**, 533–539.

24 Lin, J.-F., Struzhkin VV, Jacobsen SD, Hu MY, Chow P, Kung J, Liu H, Mao HK and Hemley RJ. 2005, *Nature* **436**, 377-380.

25 Shen, G.Y., Prakapenka, V.B., Eng, P.J., Rivers, M.L. and Sutton, S.R. 2005, Journal of Synchrotron Radiation, **12**, 642-649.

26 Hammersley, A.P., Svensson, S.O., Hanfl and, M., Fitch, A.N., and Hausermann, D. 1996, High Pressure Research, **14**, 235-248.

27 Izumi, F. and Ikeda, T. 2000, Material. Science. Forum **321–324**, 198–204.

28 Rueff, J.-P. et al. 1999, *Phys. Rev. Lett.* **82**, 3284-3287.

29 Badro, J. et al., 2003, *Science* **300**, 789-791.

30 Hahn, T. 1983, *International Tables for Crystallography, A, SpaceGroup Symmetry*.

31 Shannon, R.D. 1976, Acta Crystallographica **A32**, 751-767.

32 Crowhurst, J.C., Brown, J.M., Goncharov, A.F., & Jacobsen, S. D. 2008, *Science* **319**, 451-453.

33 Goncharov, A.F., Struzhkin, V.V., & Jacobsen, S.D. 2006, *Science* **312**, 1205-1208.

34 Ding, Y. et al., 2008. *Phys. Rev. Lett.* **100**, 045508.

35 Tsuchiya, T., Wentzcovitch, R.M., da Silva, C.R.S., and de Gironcoli, S. 2006 *Phys. Rev. Lett.* **96**, 198501-198504 (2006).